

Microscopic study of ground state bands in $N = 45$ and 46 isotones in mass region $A \sim 70$ – 80

Preeti Verma¹, Suram Singh¹ , Arun Bharti² and S K Khosa^{1,3}

¹Department of Physics and Astronomical Sciences, Central University of Jammu, Samba, J&K-(181143), India

²Department of Physics, University of Jammu, Jammu- (180001), India

E-mail: suramsingh@gmail.com

Received 23 September 2019, revised 21 January 2020

Accepted for publication 22 January 2020

Published 13 March 2020



CrossMark

Abstract

Using the angular-momentum projected quasiparticle states and a simple quadrupole–quadrupole + monopole–pairing + quadrupole–pairing type Hamiltonian, Projected Shell Model calculations have been performed to study the nuclear structure properties of some $N = 45, 46$ isotones in the mass region $A = 70$ – 80 . The results are obtained for the yrast energy spectrum, rotational alignments, back-bending and reduced transition probabilities [$B(M1)$ and $B(E2)$]. Results of our calculations exhibit satisfactory agreement with experimental data. Signature splitting and signature inversion which are the characteristics of this mass region have also been reproduced and discussed for these nuclei.

Keywords: projected shell model, yrast spectra, signature-splitting, band diagram, back-bending, reduced transition probabilities

(Some figures may appear in colour only in the online journal)

1. Introduction

Nuclei lying in the *fpg* shell having nucleon numbers between the magic numbers 28 and 50 feature many facets of elementary nuclear excitation. The presence of two closed shells and the $N = 40$ subshell makes this region of Segre's chart of particular interest for testing the nuclear models. Particularly, nuclei with $A \sim 70$ are known to be the site of a diverse set of

³ Mentor.

structural phenomena [1]. Existing research results indicate that $A \sim 70$ nuclei with the neutron number less than 44 exhibit strong collectivity whereas those with the neutron number more than 47 show single-particle excitations [2]. Nuclei which lie in between these two values, i.e. having $N = 45$ and 46, are, therefore, very important for understanding the nuclear structure evolution in this mass region. The nuclei with 45 neutrons, where the intruder $g_{9/2}$ subshell is half-filled and has already lost most of its deformation driving capability, are known to have very moderate deformations of $\beta_2 \sim 0.17$ for the rotation like positive-parity high-spin bands whereas the nuclei having 46 neutrons are expected to be even lesser deformed as one is approaching $N = 50$ shell closure. The focus of the present work is mainly on some of these $N = 45$ isotones (doubly-odd) and the neighbouring $N = 46$ isotones (odd- Z).

Doubly-odd nuclei are very interesting candidates for the nuclear structure studies as energy levels in such nuclei are most sensitive to variations of single-particle states [3]. In addition, they offer valuable information on the interplay between collective and single-neutron and -proton degrees of freedom in atomic nuclei. However, due to the complexity of their low-lying spectra studying such nuclei, both experimentally and theoretically, is quite challenging. Review of literature shows that in recent years, stimulating new data have been accumulated on the odd-odd nuclei in the $A \sim 70$ mass regions around the *pf*-shell [4–17]. This data suggest that doubly-odd nuclei with mass $A \sim 70$ exhibit a complex low spin structure which develops into a regularly spaced rotational levels above an excitation energy of 0.5–1.0 MeV. It has also been found that in this region the strong interaction between the $f_{5/2}$ protons and the $g_{9/2}$ neutrons play a crucial role [18, 19] in deciding the nuclear structure and thus, has to be taken into account while studying these nuclei. Owing to these reasons, the $A \sim 70$ doubly-odd nuclei are ideal testing grounds for different models, as their properties are extremely sensitive to the proton-neutron-interaction.

The unified theoretical description of low-lying states in even-even, odd-mass and odd-odd nuclei is one of the major goals of nuclear structure research. The microscopic description of low-lying collective states in even-even systems of the mass region $A \sim 70$ –80 has been broadly pursued with numerous theoretical methods [20–33] whereas a good amount of attempts have been made from our group [34–38] as well as some other groups [39–45] across the world to study odd-mass nuclei also. However, very little effort has been put into the theoretical front to study the doubly-odd nuclei in this mass region; this may be due to the fact that the description of odd-odd nuclei is more cumbersome, as in these systems both collective and single-particle motions have to be treated on the same footing. Also, it requires understanding of different types of coupling mechanisms of the odd-neutron and the odd-proton to the even-even core, and the Coriolis response of the neutron and proton motion to the rotation of core, and proton-neutron residual interaction in addition to the various deformation-generating mechanisms of the even-even core [46]. Although, Palit *et al* [47] have performed a systematic study of the proton-rich odd-odd nuclei in the $A \sim 70$ –80 mass region, still the doubly-odd nuclei of this mass region lack a detailed study. As our group is already involved in the nuclear structure study of even-even [29–33] and odd-mass [34–38] nuclei lying in mass 70 region within the framework of Projected Shell Model (PSM), we decided this time to explore the structure of some doubly-odd nuclei in this region using the same interaction Hamiltonian of PSM that we have used previously. In order to further check the efficacy of the PSM Hamiltonian to describe the energy spectra and other properties of doubly-odd nuclei, we have also performed the calculations on the neighbouring odd- Z nuclei having $N = 46$ using the same set of parameters as used for odd-odd nuclei.

The nuclei chosen for the present PSM study are the gallium, arsenic and bromine, having three-, five- and seven-protons, respectively, coupled to the underlying $Z = 28$ nickel

core. In particular, the ground-state properties of doubly-odd ^{76}Ga , ^{78}As and ^{80}Br (having $N = 45$) and ^{77}Ga , ^{79}As and ^{81}Br (having $N = 46$) nuclei have been described in this work. The ground-states of these nuclei are dominated by the odd-proton occupying either of the $\pi p_{3/2}$, $\pi f_{5/2}$ or $\pi p_{1/2}$ levels. In fact, the $\pi f_{5/2}$ level is found to play a dominant role in the ground state wave function of the odd-odd isotopes because of the strong $\pi f_{5/2} \nu g_{9/2}$ interaction [48]. A systematic study of these isotones can also help in investigating the deformation driving properties of the $g_{9/2}$ proton orbital in this mass region. By employing the PSM we tried to study this as well as the other nuclear structure properties like signature inversion and splitting, rotational alignments and back-bending in moment of inertia etc which are characteristics of this mass region. The brief theory of PSM is presented in section 2 of this paper whereas section 3 presents the results of the PSM calculations on various nuclear structure properties of these $N = 45$ and $N = 46$ isotones and their discussion. Finally, the results are concluded in section 4.

2. Projected shell model

The PSM [49] calculations usually begin with the deformed Nilsson single-particle states at deformation ε_2 . What one gains by starting from a deformed basis is not only that shell model calculations for heavy nuclei become feasible but also physical interpretation for the complex systems becomes easier and clearer. Pairing correlations are incorporated into these Nilsson states by BCS calculations. The consequences of the Nilsson-BCS calculations provide us with a set of quasiparticle (qp) states that define the qp vacuum $|\varphi(\varepsilon_2)\rangle = |0\rangle$ in the intrinsic frame. One then constructs the shell model bases by building multi- qp states. The broken rotational and Gauge symmetry in these states is recovered by angular momentum projection [50] and particle number projection, if necessary, to form a shell model basis in the laboratory frame. Finally, a two-body shell model Hamiltonian is diagonalized in the projected space. The last step is the configuration mixing in this much smaller projected basis. Once the Hamiltonian is diagonalized in the qp basis, the lowest energy of each spin is used to obtain yrast energy band. The resulting wave functions are usually used to compute the $B(M1)$ and $B(E2)$ transition probabilities and gyromagnetic factors (g -factor).

The chosen qp subspace for the present case of odd-odd nuclei is spanned by the basis set

$$|\phi_\kappa\rangle = \{a_{\nu_i}^\dagger a_{\pi_j}^\dagger |0\rangle\}, \quad (1)$$

where a^\dagger 's are the quasiparticle (qp) creation operators, ν 's (π 's) denote the neutron (proton) Nilsson quantum numbers which run over low-lying orbitals and $|0\rangle$ is the Nilsson + BCS vacuum (0- qp state). Each configuration in equation (1) consists of one quasineutron and one quasiproton. The indices ν and π in equation (1) are general; for example, a two- qp state can be of positive-parity if both quasiparticles i and j are from the same major \mathbf{N} shell, or of negative parity if i and j are from \mathbf{N} shells differing by $\Delta\mathbf{N} = 1$. For the current odd-odd nuclei, low-lying two- qp states with positive-parity are those in which both the neutron and the proton occupy the $\mathbf{N} = 4$ fpg shell. The configuration space is obviously large in this case compared to the nearby odd-mass nuclei and usually several configurations contribute to the shell model wave function of a state with nearly equal weightage. This makes the numerical results very sensitive to the shell filling and the theoretical predictions for doubly-odd nuclei become far more challenging.

For odd- Z nuclei, configuration space is spanned by the basis set

$$|\phi_\kappa\rangle = \{a_\pi^\dagger|0\rangle, a_\pi^\dagger a_{\nu_1}^\dagger a_{\nu_2}^\dagger|0\rangle\}, \quad (2)$$

where, the low-lying 3- qp states selected for the many-body basis are those consisting of 1- qp (*quasiproton*) plus a pair of qp 's from nucleons of another kind (*quasineutrons*). This selection is based on physical considerations. In general, 3- qp states made by three nucleons of the same kind are also allowed, but such states usually lie higher in energy and, therefore, are not included. The inclusion of the 3- qp configurations is important for odd-mass nuclei for a description of the band-crossing phenomenon which is caused by a rotation alignment of a pair of quasineutrons.

In the PSM, the many-body wave function is a superposition of (angular momentum) projected multi-quasiparticle states; Angular momentum projection transforms the wave function from the intrinsic frame to the laboratory frame. The total wave function is expressed as

$$|\Psi_{IM}^\sigma\rangle = \sum_{K\kappa} f_\kappa^\sigma \hat{P}_{MK}^I |\phi_\kappa\rangle \quad (3)$$

with

$$\hat{P}_{MK}^I = \frac{2I+1}{8\pi^2} \int d\Omega D_{MK}^I(\Omega) \hat{R}(\Omega), \quad (4)$$

where, the index σ labels the states with same angular momentum and κ labels the basis states. \hat{P}_{MK}^I is the angular momentum projection operator and f_κ^σ are the weights of the basis state κ . The energies and wave functions (given in terms of the coefficients f_κ^σ in equation (3)) are obtained by solving the following eigen-value equation:

$$\sum_{\kappa'} \{H_{\kappa\kappa'}^I - E_I N_{\kappa\kappa'}^I\} f_{\kappa'}^\sigma = 0, \quad (5)$$

where, $H_{\kappa\kappa'}^I$ and $N_{\kappa\kappa'}^I$ are, respectively, the matrix elements of the Hamiltonian and the norm and are given as

$$H_{\kappa\kappa'}^I = \langle \phi_\kappa | \hat{H} \hat{P}_{K\kappa'}^I | \phi_{\kappa'} \rangle \text{ and } N_{\kappa\kappa'}^I = \langle \phi_\kappa | \hat{P}_{K\kappa'}^I | \phi_{\kappa'} \rangle. \quad (6)$$

The projection of an intrinsic state $|\phi_k\rangle$ on a good angular momentum generates a rotational energy of a band (or the band energy)

$$E_\kappa(I) = \frac{\langle \phi_\kappa | \hat{H} \hat{P}_{K\kappa}^I | \phi_\kappa \rangle}{\langle \phi_\kappa | \hat{P}_{K\kappa}^I | \phi_\kappa \rangle} = \frac{H_{\kappa\kappa}^I}{N_{\kappa\kappa}^I} \quad (7)$$

which can be plotted as a function of spin for various bands and important physics can be drawn from these plots.

The Hamiltonian appearing in equations (5)–(7) is the usual PSM Hamiltonian which consists of the harmonic oscillator single-particle Hamiltonian and a sum of schematic (quadrupole–quadrupole ($Q\cdot Q$) + Monopole Pairing + Quadrupole Pairing) forces. These forces represent specific correlations fundamental for nuclear structure. The Hamiltonian is of the form

$$\hat{H} = \hat{H}_0 - \frac{1}{2} \chi \sum_\mu \hat{Q}_\mu^\dagger \hat{Q}_\mu - G_M \hat{P}^\dagger \hat{P} - G_Q \sum_\mu \hat{P}_\mu^\dagger \hat{P}_\mu, \quad (8)$$

where \hat{H}_0 is the spherical single-particle Hamiltonian which in particular contains a proper spin–orbit force, whose strengths (i.e. the Nilsson parameters κ and μ) are taken from [51].

This single-particle term is given by

$$\hat{H}_0 = \sum_{\alpha} c_{\alpha}^{\dagger} E_{\alpha} c_{\alpha}, \quad (9)$$

where c_{α}^{\dagger} and c_{α} are the single-particle creation and annihilation operators, respectively, and E_{α} is the single-particle energy given by

$$E_{\alpha} = \hbar\omega[N - 2\kappa\hat{l}\cdot\hat{s} - \kappa\mu(\hat{l}^2 - \langle\hat{l}\rangle^2)]. \quad (10)$$

The second term in the Hamiltonian (8) is the $Q.Q$ interaction and the last two terms, the monopole and quadrupole pairing interactions, respectively. The interaction strengths are determined as follows:

- The $Q.Q$ interaction strength χ is adjusted by the self-consistent relation such that the input quadrupole deformation ε_2 and the one resulting from the HFB procedure coincide with each other.
- The monopole pairing strength G_M is taken to be $G_M = \left(G_1 \pm G_2 \frac{N-Z}{A}\right) \frac{1}{A}$ with ‘+ (−)’ is for protons (neutrons), which was first introduced by Dieterich *et al* [52]. The choice of the strengths G_1 and G_2 depends on the size of the single-particle space in the calculation. Here, in the present case, G_1 and G_2 are taken as 20.20 MeV and 12.12 MeV for both doubly-odd and odd- Z nuclei.
- Finally, the quadrupole pairing strength G_Q is assumed to be proportional to G_M , and is set as about 1/5th of the monopole pairing constant, G_M , allowing a $\pm 10\%$ variation to adjust the position of back-bending. The value of G_Q in the present case is set to be 0.16 times G_M .

It should also be noted that in the present calculations, the configuration space contains three major shells, $N = 2, 3, 4$ for protons and $N = 3, 4, 5$ for neutrons. Moreover, $Z = 8$ and $N = 20$ are taken as inert cores for protons and neutrons, respectively.

The Shell model space in the present calculations is truncated at a deformation, $\varepsilon_2 = 0.195$, for all the nuclei under study which is very close to the values given in [8, 53–55]. This truncation is achieved by the inclusion of the states within an energy window of 6.5 MeV around the Fermi surface. This determines the size of the basis space, $|\phi_k\rangle$ in equations (1) and (2) of the order of 30.

By applying PSM approach, one can study various nuclear structure properties such as yrast energies, band diagrams, rotational frequencies, electromagnetic transitions, etc. Electromagnetic transitions can give important information on the nuclear structure, thereby enhancing our knowledge of nuclear structure. Electromagnetic properties play an instrumental role in the critical evaluation of various models. In the present work, we have calculated the electromagnetic properties using the PSM wave functions. The reduced electric quadrupole transition probability $B(E2)$ from an initial state ($I_i = I$) to a final state ($I_f = I - 2$) is given by [56]

$$B(E2, I \rightarrow I - 2) = \frac{e^2}{2I + 1} |\langle \psi^{I-2} || \hat{Q}_2 || \psi^I \rangle|^2 \quad (11)$$

Here we are interested in $E2$ transitions from $I_i = I$ to $I_f = I - 2$; therefore the operator \hat{Q}_2 is related to the quadrupole operator by

$$\hat{Q}_{2\nu} = e_{\nu}^{\text{eff}} \sqrt{\frac{5}{16\pi}} Q_{\nu}^2, \quad \hat{Q}_{2\pi} = e_{\pi}^{\text{eff}} \sqrt{\frac{5}{16\pi}} Q_{\pi}^2. \quad (12)$$

The standard values of effective charges which are used in these expression are $e_\nu^{\text{eff}} = 0.5e$ for neutrons and $e_\pi^{\text{eff}} = 1.5e$ for protons. However, one may adjust these values of effective charges to take into consideration the effects of core polarization. It may be also be noted that any variations in calculated $B(E2)$'s among one rotational band or between those in different nuclei, are subject to the structure change in wave functions.

Similarly, one can calculate reduced magnetic transition probability using PSM wave functions. Magnetic dipole transition strengths are sensitive to the single-particle attributes of the nuclear wave function, The reduced magnetic dipole transition probability $B(M1)$ is computed by

$$B(M1, I \rightarrow I - 1) = \frac{\mu_N^2}{2I + 1} |\langle \psi^{I-1} | \hat{M}_1 | \psi^I \rangle|^2, \quad (13)$$

where the magnetic dipole operator is defined as

$$\hat{M}_1^\tau = g_l^\tau \hat{j}^\tau + (g_s^\tau - g_l^\tau) \hat{s}^\tau \quad (14)$$

here τ is either π or ν , and g_l and g_s are the orbital and the spin gyromagnetic factors, respectively. The standard free values of g_l and g_s for protons and neutrons are

$$g_l^\pi = 1, \quad g_l^\nu = 0, \quad g_s^\pi = 5.586, \quad \text{and} \quad g_s^\nu = -3.826$$

however, in the PSM calculations, the free values of g_l^π and g_l^ν are used, whereas g_s^π and g_s^ν are generally damped by a usual 0.75 factor from the free-nucleon values to account for the core-polarization and meson-exchange current corrections [57].

Since the configuration space is large enough we do not use any core contribution. The reduced matrix element of an operator \hat{O} (\hat{O} is either \hat{Q} or \hat{M}) is expressed by

$$\begin{aligned} \langle \psi^{I_f} | \hat{O}_L | \psi^{I_i} \rangle &= \sum_{\kappa_i, \kappa_f} f_{I_i \kappa_i}^{\sigma_i} f_{I_f \kappa_f}^{\sigma_f} \sum_{M_i, M_f, M} (-1)^{I_f - M_f} \\ &\times \begin{pmatrix} I_f & L & I_i \\ -M_f & M & M_i \end{pmatrix} \\ &\times \langle \phi_{\kappa_f} | \hat{P}_{K_{\kappa_f} M_f}^{I_f} \hat{O}_{LM} \hat{P}_{K_{\kappa_i} M_i}^{I_i} | \phi_{\kappa_i} \rangle. \end{aligned} \quad (15)$$

3. PSM results

3.1. Yrast levels

Yrast bands up to the spin of $16\hbar$ for ^{76}Ga , ^{78}As and ^{80}Br are calculated and plotted and compared with the available experimental data in figures 1(a)–(c). The experimental data for these isotones are taken from NNDC database [15–17] and [8]. On analysing this available data we found that in case of ^{76}Ga , the ground state band is a positive-parity with band-head at 2^+ and maximum known spin of 3^+ . The spin and parity assignment of the energy levels in ^{76}Ga are tentative and nearly degenerate spin and parities have been predicted for the low lying states. The NNDC data lists $(2^+, 3^+)$ for the spin, parity of the ground state in this nucleus, while Mane *et al* [4] preferred a 2^- assignment for the ground state based on the measurement of magnetic moment in accordance with the shell Model calculations. The next higher experimental state which is situated at energy of 0.172 MeV is again found to be degenerate state $(1^+, 2^+, 3^+)$. However, for our reference, we have taken 2^+ as the ground state and 3^+ as the excited state in this nucleus. In case of ^{78}As , the ground state band is found to have negative-parity with band-head at 2^- whereas the maximum observed spin is 6^- in

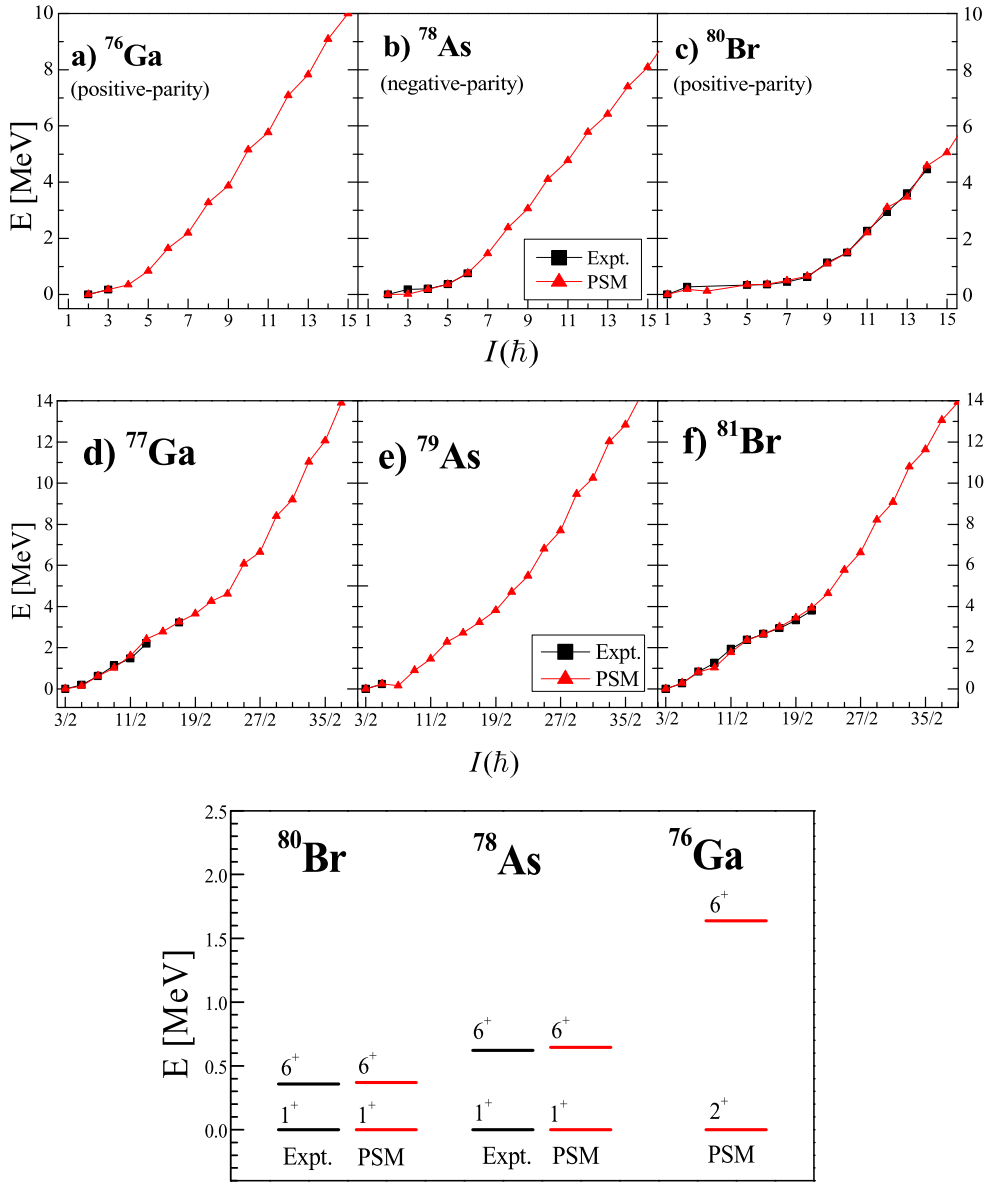


Figure 1. (a)–(f) Comparison of calculated (PSM) yrast energy states with available experimental (Expt.) data for (a) ^{76}Ga [15], (b) ^{78}As [16], (c) ^{80}Br [17], (d) ^{77}Ga [58], (e) ^{79}As [59], (f) ^{81}Br [60]. (g) Systematics of the 6^+ state in $N = 45$ isotones.

this nucleus. The ground state band is again a positive-parity band in case of ^{80}Br , with band-head at 1^+ and experimental data is available up to the maximum spin of 14^+ .

Our PSM calculations predict the ground state in ^{76}Ga to have the spin-parity of 2^+ whereas the next higher calculated energy level (with energy 0.171 MeV) is predicted to have spin-parity of 3^+ . This result and other higher calculated states are shown in figure 1(a) in comparison with the experimental data. If we take the case of ^{78}As and ^{80}Br , PSM

calculations favour the ground state band-heads at $K^\pi = 2^-$ and 1^+ , respectively, which are in agreement with the experimental data. Further, from figures 1(a)–(c), it is clear that the calculated PSM data reproduced the available experimental data with a satisfactory degree of agreement where the maximum gap between the experimental and the calculated energy levels is ~ 0.2 MeV in case of ^{78}As for 3^- state. One may note that due to the scarcity of experimental data at higher spins, we have plotted the PSM data up to the spin of $16\hbar$ only, though we were able to obtain higher energy levels owing to the alignment of 2-quasiparticles in the *fpg* configuration space.

For the odd- Z $N = 46$ isotones, PSM results are plotted and compared with the experimental data [58–60] in figures 1(d)–(f). The bandhead of ground state bands in these isotones, ^{77}Ga , ^{79}As and ^{81}Br , is $3/2^-$ having negative-parity. Further, in ^{77}Ga , the experimental data is available up to the maximum spin of $17/2^-$ whereas in case ^{79}As only one excited state is observed having $K^\pi = 5/2^-$. In ^{81}Br , high energy states up to $21/2^-$ are available experimentally. The PSM calculations for these odd- Z isotopes are performed by making use of the same set of input parameters as was used for odd–odd isotones. The PSM data is obtained up to the spin of $51/2^- \hbar$ for these isotones however in figure 1 we have plotted the energy levels up to the spin $35/2^-$ only as experimental data is not available for comparison at higher spins. The experimental data, whatsoever available, is reproduced with a satisfactory degree of agreement by the PSM calculations which prove the efficacy of the set of input parameters used in the PSM Hamiltonian to give a unified description of the nuclear structure in this mass region.

It is noted by Doring *et al* [7] that with the decrease in number of protons, i.e. while going from ^{82}Rb to ^{78}As , the low-lying 6^+ state moves from 191 keV in ^{82}Rb to 357 keV in ^{80}Br to 621.9 keV in ^{78}As , exhibiting the fact that the filling of the $g_{9/2}$ proton orbital becomes energetically more expensive. In the present PSM calculations, we found that 6^+ state in ^{80}Br occurs at 370.7 KeV whereas in ^{78}As it is found to have the energy 644 KeV. As we further move to ^{76}Ga , this 6^+ state is found to get further pushed up to energy of 1637.7 KeV. These results (see figure 1(g)) supports the findings of Doring *et al* and also points out that the $g_{9/2}$ proton orbital does not play much significant role for the low-lying states in these isotones, thereby, resulting in a less deformed nuclei.

3.2. Quasi-particle structure of $N = 45$ and $N = 46$ isotones

Band diagrams can bring valuable information regarding the underlying physics and depict the results of the projected energies for each intrinsic configuration. These band diagrams for the studied odd–odd $N = 45$ Ga, As, and Br isotones are presented in figures 2(a)–(c) and for odd- Z , $N = 46$ Ga, As, and Br isotones in figures 2(d)–(f). In the diagrams for odd–odd isotones, the projected energies are shown for two quasiparticle configurations (with $K = K_\nu \pm K_\pi$) whereas for odd- Z isotones, three quasiparticle configurations (one quasi-proton plus a pair of quasineutrons) are shown. In these figures, the projected bands (which are unperturbed rotational bands), obtained from the axially deformed intrinsic Nilsson state by performing the angular-momentum projection, are displayed, i.e. the expectation value of Hamiltonian and the coupling between the various bands is not taken into account.

The yrast energies obtained by the final shell model diagonalization are also plotted in these figures so that one can have an explicit idea about the quasiparticle configurations contributing towards the formation of yrast spectra at different angular momenta in these nuclei. Further, it may be noted that as many as 38 bands have been obtained in the calculations but only those bands have been plotted in the band diagrams that lie low in energy as only these bands are important from physics point of view. It is quite clear from these figures

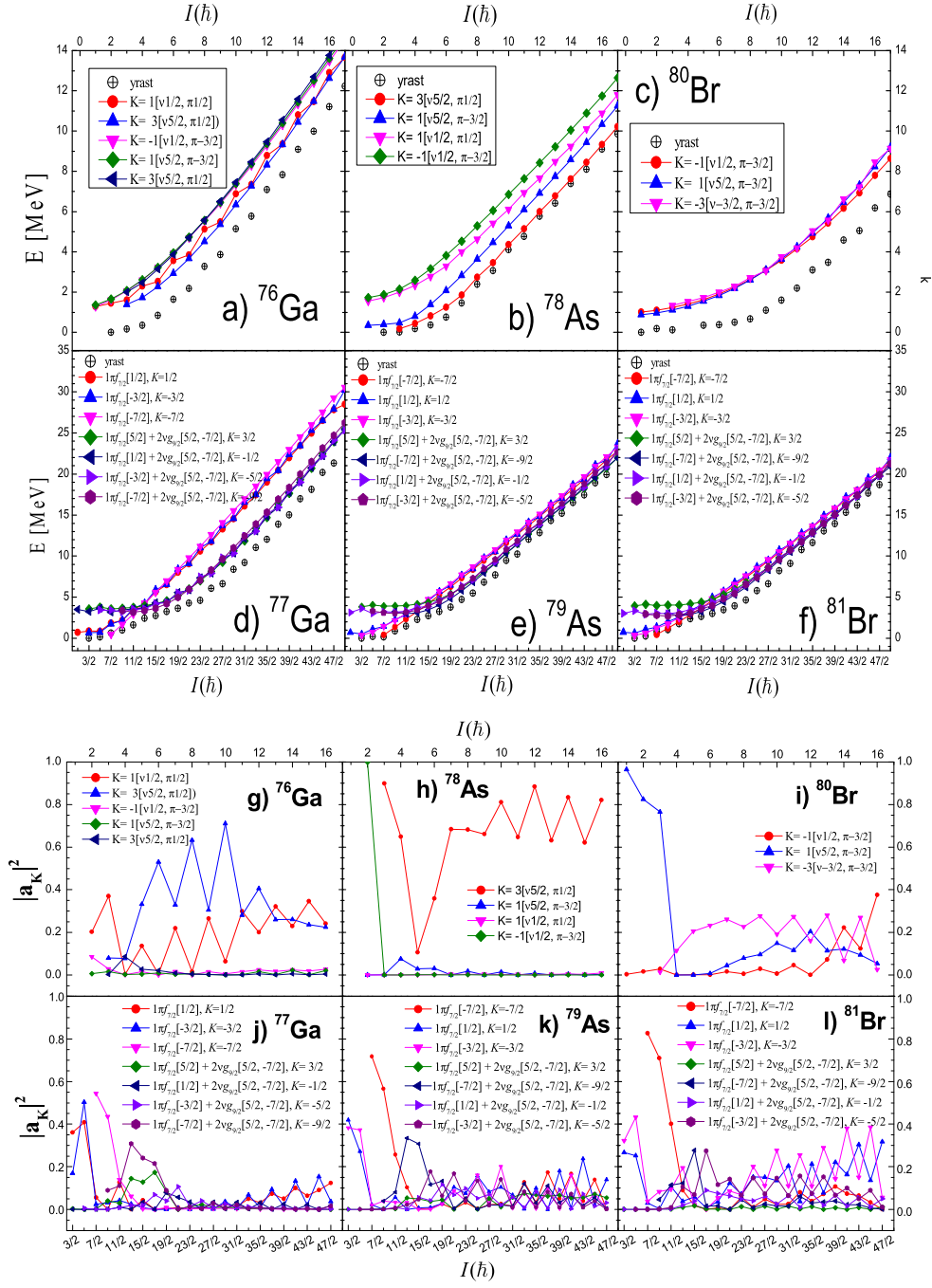


Figure 2. (a)–(f) Band diagrams for (a) ^{76}Ga , (b) ^{78}As , (c) ^{80}Br , (d) ^{77}Ga , (e) ^{79}As , (f) ^{81}Br . (g)–(l) Probability amplitude of various projected K -configurations in the wave functions of the yrast bands for $N = 45$ isotones (g)–(i) and $N = 46$ isotones (j)–(l).

that all the band diagrams reflect same nature of uniformly increasing bands in energy for the studied odd-odd nuclei in $A \sim 70$ region.

In case of ^{76}Ga , there are five 2-*qp* bands with band heads 0^+ , 1^+ , 2^+ , 3^+ , 4^+ lying very close to each other in energy gap of ~ 1.5 MeV which interact with each other to give rise to the yrast band in this nucleus so that the yrast levels have composite structure. These bands are obtained by specifying K -values in the angular-momentum projection operator. It is noted that in ^{76}Ga , the quasi-neutron band is either arising from the $p_{3/2}$ or $f_{5/2}$ whereas the quasiproton bands are arising from the $f_{5/2}$ orbital. Similarly, in ^{78}As , the contribution towards the formation of yrast band comes primarily from four low-lying bands with $K^\pi = 3^-, 1^-, 1^-$ and 4^- (see figure 2(b)) out of which one 2-*qp* band having configuration $K = 3[\nu 5/2, \pi 1/2]$ is dominating. Here, in this case, the bands are negative parity bands where the quasineutron bands are from the $g_{9/2}$ orbital and quasi-proton band are coming from $f_{5/2}$. This is in accordance with the previous works [7, 61] where the ground state in this nucleus was ascribed to the $(\pi f_{5/2} \otimes \nu g_{9/2})$ 2-*qp* configuration. Next, in case of ^{80}Br , three 2-*qp* bands with configurations $|K| = 1[\nu 1/2, \pi - 3/2]$, $|K| = 1[\nu 5/2, \pi - 3/2]$ and $|K| = 3[\nu - 3/2, \pi - 3/2]$ are lying very close to each other and almost overlapping to give rise to the yrast spectra in this nucleus. Both the quasineutron and quasiproton bands in this case are originating from the $g_{9/2}$ orbital to give rise to the 2-*qp* positive parity bands. Experimentally also, the high-spin states of positive parity in ^{80}Br are ascribed to the intruder two-quasiparticle $(\pi g_{9/2} \otimes \nu g_{9/2})$ configuration [5, 6].

In all these $N = 45$ isotones, composite structures due to mixing of bands is predicted. Moreover, the change in the band-heads as well as the parity on the addition of two protons while going from Ga to As to Br is understood to occur due to the change in the energies of the $f_{5/2}$, $g_{9/2}$ proton orbitals and $p_{3/2}$, $f_{5/2}$ and $g_{9/2}$ neutron orbitals.

Taking the case of $N = 46$ isotones, yrast states built on the 3-*qp* bands having the configuration of one quasiproton and two quasineutrons have been predicted (figures 2(d)–(f)). Let us first take the case of ^{77}Ga . In this isotope, the low spin yrast states are generated by mixture of two 1-*qp* quasiproton bands $1\pi f_{7/2} [1/2]$, $1\pi f_{7/2} [-3/2]$ up to the spin of $5/2^-$ whereafter it is overtaken by another 1-*qp* band having configuration $1\pi f_{7/2} [-7/2]$ and this constitutes the yrast spectra up to $I = 11/2^-$. A 3-*qp* band identified as $1\pi f_{7/2} [-7/2] + 2\nu g_{9/2} [5/2, -7/2]$, $|K| = 9/2$ crosses this 1-*qp* band just after the spin $11/2^-$. A mixture of three other 3-*qp* bands with configurations $1\pi f_{7/2} [5/2] + 2\nu g_{9/2} [5/2, -7/2]$, $|K| = 3/2$, $1\pi f_{7/2} [1/2] + 2\nu g_{9/2} [5/2, -7/2]$, $|K| = -1/2$ and $1\pi f_{7/2} [-3/2] + 2\nu g_{9/2} [5/2, -7/2]$, $|K| = 5/2$ are very close to this crossing band with $|K| = 9/2$ which ultimately become slightly lower than the $|K| = 9/2$ band after the spin of $27/2^-$ and give rise to the higher spin yrast states. A similar trend is seen in ^{79}As also, where the low spin yrast states are arising from the contribution from three 1-quasiproton bands with $|K| = 7/2, 1/2$ and $3/2$. Band crossing in this case, as predicted by PSM calculations, occurs at $13/2^-$ and the band responsible for this crossing is identified as 3-*qp* band consisting of $f_{7/2} [-7/2]$ quasiproton and a pair of quasineutrons $g_{9/2} [5/2, -7/2]$. However, here also, this 3-*qp* band lies very close to the mixture of another three 3-*qp* bands with band-heads $|K| = 3/2, 1/2$ and $5/2$ and interaction of these four bands are predicted to produce the high spin yrast states in this nucleus [figure 2(e)]. Things are quite similar in ^{80}Br , where again the low spin yrast states are arising from the contribution from three 1-quasiproton bands with $|K| = 7/2, 1/2$ and $3/2$. These bands are crossed by 3-*qp* band having configuration $1\pi f_{7/2} [-7/2] + 2\nu g_{9/2} [5/2, -7/2]$, $|K| = 9/2$ which is almost degenerate with three other 3-*qp* bands (see figure 2(f)).

In case of these $N = 46$ isotones apart from predicting the multi-quasiparticle (3-*qp*) structure of yrast states at higher spins, PSM calculations also point out that the quasiproton bands are from the $f_{7/2}$ orbital whereas the quasineutron bands originates from the $g_{9/2}$ orbital.

In the PSM approach, the eigenvalues of energy along with the amplitude of wave functions are obtained by diagonalization of the total Hamiltonian. The schematic analysis of the probability amplitude of various n - qp configurations *versus* spin for $N = 45$ and $N = 46$ isotones are displayed in figures 2(g)–(l), respectively. It is to be noted that we have plotted the probability amplitude for those configurations only which are contributing significantly towards the formation of yrast band as clear from the band diagrams. For $N = 45$ isotones, only 2- qp configurations are involved. In case of ^{76}Ga , the probability amplitude has the dominant $K = 1$ and 3 configurations for the whole spin range whereas in ^{78}As , the dominant configuration for the formation of the yrast band is that with $K = 3$ with some contribution from $K = -1$ and $K = 1$ configurations at low spins. For ^{80}Br , at low spins $K = 1$ band is dominating and after that significant contribution is coming from the $K = -3$ configuration along with this $K = 1$ configuration. Further, on carefully analysing the wavefunctions obtained for these $N = 45$ isotones we have found that $g_{9/2}$ proton orbital plays either no or very less significant role especially at lower spins in these isotones which is again in accordance with the results of Doring *et al* [7].

In case of $N = 46$ isotones, it is clear from the probability amplitude plots that the lower spins of the yrast bands have major contribution from the 1- qp configurations whereas after the spin of $11/2^-$, 3- qp configurations become dominating. This kind of behaviour is already revealed from the band diagrams of these $N = 46$ isotones where 1- qp bands are crossed by the 3- qp bands to give rise to the yrast states at mid- and higher- spin range.

3.3. Signature splitting and inversion in $N = 45$ isotones

Experimentally, one often observes an energy staggering in rotational bands and refer to this as signature-splitting. Energy signature-splitting is basically the shift between the energetically favoured and the unfavoured sequences of levels. However, whenever an expected favoured branch (lower in energy) becomes unfavoured at higher spins, it is known as signature-inversion. Both these phenomena have attracted a lot of research focus both at experimental and theoretical fronts in the recent past. The nuclei in the mass 70 region are found to exhibit both these phenomena. It has been pointed out [7] earlier that the signature inversion in the mass 70–80 region is related to the filling of the high- j $g_{9/2}$ proton and $g_{9/2}$ neutron subshells and reflects the transition from mainly single-particle excitations at low spins to more rotational (collective) motion at higher spins. The signature splitting and inversion are best understood by plotting the quantity $[E(I) - E(I-1)]/2I$ as a function of the spin I of the initial state [62]. The plot of $[E(I) - E(I-1)]/2I$ versus I for the $N = 45$ and $N = 46$ isotones are shown in figures 3(a)–(f), respectively.

For the $N = 45$ isotones, one sees from the figures that the signature splitting is very much present at the middle and higher spin range in these nuclei, where the odd-spin states are lower in energy while the even spin states are higher in energy except for ^{80}Br . In case of ^{80}Br , even-spin states are lower in energy in the low-spin region while the energy difference of odd-spin states becomes lower after the reversal in the phase of the staggering (signature inversion) takes place in this nucleus at the spin $I = 12\hbar$. Experimentally also a signature inversion is observed in ^{80}Br at the spin of $12\hbar$ [8] where the yrast band is found to be composed of two bands, Bands 1a and 1b which are identified as the $\alpha = 0$ and $\alpha = 1$ signature partners, respectively, built upon the 0.331 MeV state. Things are quite different in case of ^{76}Ga and ^{78}As , where an inversion in the staggering pattern is seen in the low-spin range (at spins 5^+ and 5^- in ^{76}Ga and ^{78}As , respectively). While the experimental data is not reported for ^{76}Ga , the trend shown by experiments in ^{78}As is satisfactorily reproduced by the PSM calculations in this nucleus. It may be pointed out here that signature inversion in the vicinity of $11\hbar$ is a commonly observed feature in the positive-parity yrast bands of odd–odd nuclei in this mass 70 region, and it is indicative of an

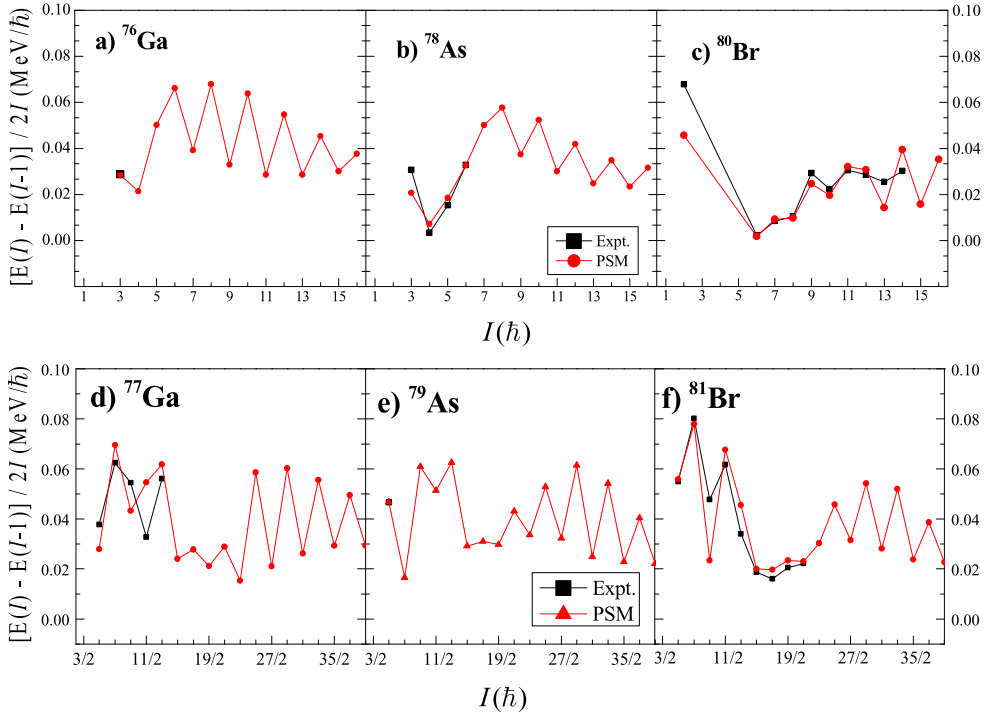


Figure 3. (a)–(c) Plots of the quantity $(E(I) - E(I - 1))/2I$ as a function of spin I for the yrast bands in $N = 45$ isotones. (d)–(f) Plots of the quantity $(E(I) - E(I - 1))/2I$ as a function of spin I for the yrast bands in $N = 46$ isotones.

underlying $\pi g_{9/2} \otimes \nu g_{9/2}$ quasi-particle configuration [13] and results of our calculations also corroborate this as may be seen for ^{80}Br .

For the negative-parity yrast band in $N = 46$ isotones, figures 3(d)–(f) show the presence of signature-splitting in these. It is noted from the figure that the features of the quantity $[E(I) - E(I - 1)]/2I$ are quite similar among these three nuclei, i.e. the magnitude of the signature splitting is larger in the beginning then decrease in the mid-spin range (from $15/2^-$ to $21/2^-$) and then again increases at the higher spins. Further, in case of ^{77}Ga , signature inversion is found to occur experimentally at $I = 9/2^-$ while PSM calculations predict it with a delay, i.e. at the spin of $11/2^-$. In ^{79}As , our PSM calculations do not predict any inversion of the signature while the experimental data is not reported beyond $5/2^-$, so one cannot comment on the presence of this feature in ^{79}As . Talking about ^{81}Br , the experimental trend of the signature splitting is very well reproduced by the PSM calculations (see figure 3(f)). Signature is found to invert at the spin of $13/2^-$ in this nucleus both experimentally and theoretically. It may also be noted that with the proton number increasing from 31 to 35, the signature inversion gets delayed.

3.4. Rotational features of $N = 45$ and $N = 46$ isotones (alignments and kinematical and dynamical moments of inertia)

The complete description of rotating nuclei not only depends on the deformations of nuclei but also on the energies and alignment properties of the single-particle orbits in them. It has been observed that in rotational nuclei there is a rapid increase of the moment of inertia with the decrease in the rotational frequency at a particular value of spin: the *phenomenon known*

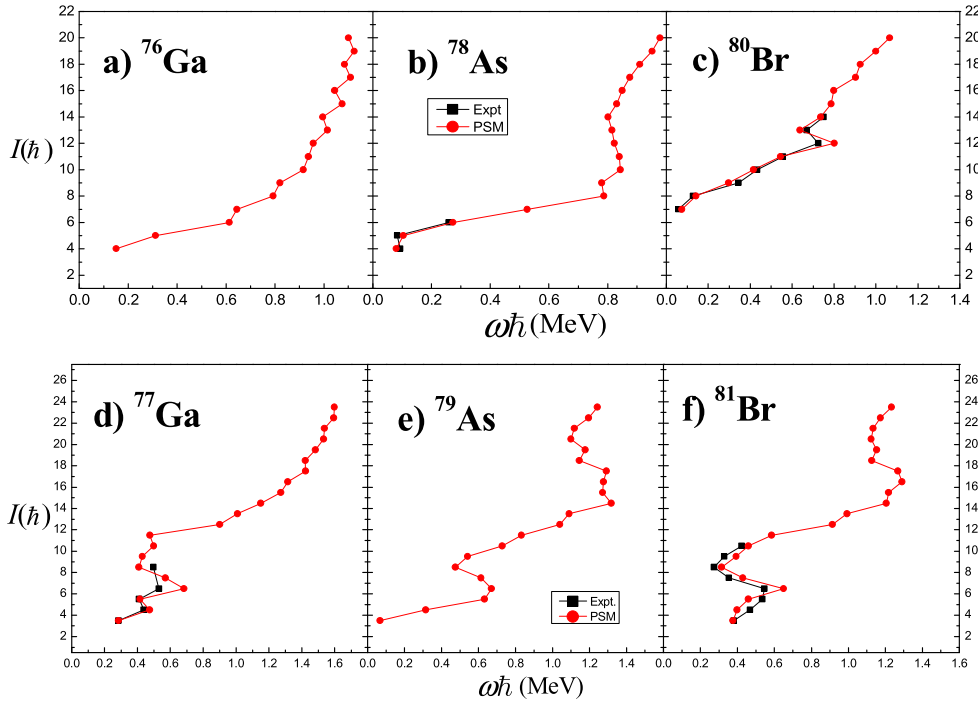


Figure 4. (a)–(c) Alignment diagrams for the yrast bands in $N = 45$ isotones, where the rotational frequency ω is plotted against spin I . (d)–(f) Alignment diagrams for the yrast bands in $N = 46$ isotones, where the rotational frequency ω is plotted against spin I .

as *backbending*. The variation and back-bending in moments of inertia correspond to rotation alignments of quasiparticles in particular orbitals along the axis of rotation.

The alignment plots for $N = 45$ isotones are presented in figures 4(a)–(c) whereas figures 5(a)–(c) and 6(a)–(c) represents the $\mathcal{J}^{(1)}$ and $\mathcal{J}^{(2)}$ plots, respectively.

The quantities, kinematical moment of inertia, $\mathcal{J}^{(1)}$, dynamical moment of inertia, $\mathcal{J}^{(2)}$, and rotational frequency, $\hbar\omega$, are defined as

$$2\mathcal{J}^{(1)} = \frac{(2I - 1)}{\omega}, \quad (16)$$

$$\mathcal{J}^{(2)} = \frac{4}{E_\gamma(I) - E_\gamma(I - 2)} \quad (17)$$

and

$$\hbar\omega = \frac{E_\gamma}{\sqrt{(I + 1)(I + 2) - K^2} - \sqrt{(I - 1)I - K^2}}, \quad (18)$$

where, the transition energy $E_\gamma = E(I) - E(I - 2)$ and $\omega = E_\gamma/2$.

The alignment plots for $N = 45$ isotones are presented in figures 4(a)–(c). In case of ^{76}Ga and ^{78}As , due to lack of experimental data or other theoretical data, only PSM results are presented. The PSM results predict alignments at $\hbar\omega \sim 1.01$ MeV and 0.80 MeV for ^{76}Ga and ^{78}As , respectively. For ^{80}Br , our PSM calculations predict the occurrence of alignment at $\hbar\omega \sim 0.8$ MeV whereas cranking model analysis of the experimental data obtained by

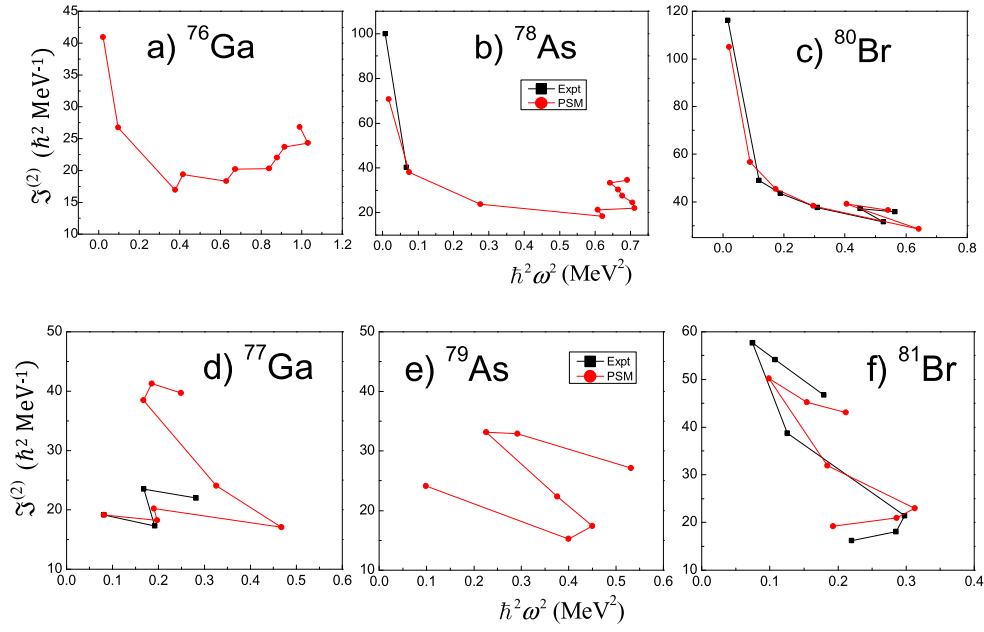


Figure 5. (a)–(c) Twice the kinetic moment of inertia, $2\mathcal{J}^{(1)}$, plotted against angular frequency squared ($\hbar^2\omega^2$) in comparison with the experimental data for yrast bands in $N = 45$ isotones. (d)–(f) Twice the kinetic moment of inertia, $2\mathcal{J}^{(1)}$, plotted against angular frequency squared ($\hbar^2\omega^2$) in comparison with the experimental data for yrast bands in $N = 46$ isotones.

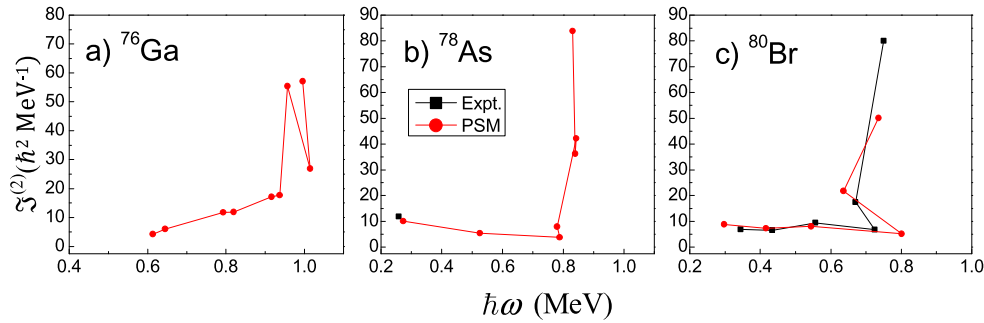


Figure 6. (a)–(c) Experimental and theoretical dynamical Moment of inertia plotted against $\hbar\omega$ for $N = 45$ isotones.

Ray *et al* [8] revealed a probable neutron alignment at $\hbar\omega \sim 0.7$ MeV in this nucleus. However, both experimental and theoretical alignments are found to occur at the same angular momentum and the overall trend of the experimental data is very well reproduced by PSM results for ^{80}Br .

Another important observation made here is that in the alignment plot of ^{76}Ga , there is a zigzag behaviour of the rotational frequency after the spin $12\hbar$ whereas this is not the case for the other two $N = 45$ isotones. This staggering in case of ^{76}Ga is understood to occur because of the mixing of the lower $K = 3$ [$\nu 5/2, \pi 1/2$] band with the $K = 1$ [$\nu 1/2, \pi 1/2$] band

which have a zigzag variation of the energy (see figure 2(a)). However, in ^{78}As and ^{80}Br , no such staggering band is found to occur.

PSM Results obtained for the kinematical ($\mathcal{J}^{(1)}$) and dynamical ($\mathcal{J}^{(2)}$) moments of inertia for these $N = 45$ isotones are presented in figures 5(a)–(c) and 6(a)–(c), respectively. One may note that behaviour of the dynamical moment of inertia $\mathcal{J}^{(2)}$ in doubly-odd nuclei is a strong indicator of the nuclear structure, particularly with regard to signature splitting of the bands. Again the experiment data is sparse for ^{76}Ga and ^{78}As however, in case of ^{80}Br , the PSM results are seen to reproduce experimentally observed back-bending in moment of inertia at the same spin but at slightly higher frequency. Moreover, in the present set of $N = 45$ isotones under study, the $\mathcal{J}^{(1)}$ values are found to be large at low rotational frequencies and then, to converge to the rigid body value of $\sim 20 \hbar^2 \text{MeV}^{-1}$. Similarly, the dynamical moment of inertia values are also positioned close to the rigid body value up to $\hbar\omega \sim 0.6 \text{ MeV}$. These results indicates a quasirigid rotation in these $N = 45$ doubly-odd isotones. Also, the dynamical moment of inertia values ($\mathcal{J}^{(2)}$) are found to increase with rotational frequency which is indicative of the onset of nucleon alignment in these nuclei as the rotational frequency increases.

For $N = 46$ isotones, results on alignments and the kinematical ($\mathcal{J}^{(1)}$) moments of inertia are presented in figures 4(d)–(f) and 5(d)–(f), respectively. For such odd-mass nuclei these processes are phenomenologically associated with crossings between bands with 1- and 3- qp configurations. Experimentally, the rotational alignment in case of ^{77}Ga is found to occur at $\hbar\omega = 0.43 \text{ MeV}$ corresponding to the spin $9/2^-$ however our PSM calculations predicts it at $\hbar\omega = 0.65$ (but at same spin). In case of ^{79}As , PSM results predict the alignment at $\hbar\omega \sim 0.6 \text{ MeV}$ corresponding to spin $13/2^-$ however, no experimental data is reported to make comparison. Lastly, in ^{81}Br , both experiment and PSM results predict the alignment at $13/2^-$ however, the rotational frequency at which this alignment occur is found to be $0.55\hbar\omega$ [MeV] experimentally and $0.65 \hbar\omega$ [MeV] through PSM calculations. It is noteworthy that in these $N = 46$ isotones, the band crossing between the 1- qp and the 3- qp bands are predicted at the spin of $11/2^-$ for ^{77}Ga and $13/2^-$ for ^{79}As and ^{81}Br (see 3.2 for details). So, one may conclude that the PSM results on band crossing are also in satisfactory agreement with the observations of the experiments for these nuclei except for ^{77}Ga where PSM predicted a delayed crossing at $11/2^-$ against the experimental $9/2^-$ which may be due to the improper band mixing at this spin. If we talk about the kinematical ($\mathcal{J}^{(1)}$) moment of inertia, not much experimental data is reported for ^{77}Ga and ^{79}As while good amount of data is made available by the experiments for ^{81}Br . The trends of the experimental data, whatever reported, are very well reproduced by the PSM results for these nuclei. The theoretical back-bendings are found to be occurring at the same spins at which the experimental back-bendings are found to occur. Moreover, two back to back backbendings in kinematical moment of inertia in case of ^{81}Br are also satisfactorily reproduced by the PSM data.

3.5. Reduced transition probabilities

Reduced transition probabilities, $B(E2)$'s and $B(M1)$'s, have been calculated for the yrast band in $N = 45$ and $N = 46$ isotones using the PSM wave-functions according to equations (11) and (13). The results are presented in presented in tables 1 and 2, respectively, for $B(M1)$'s and $B(E2)$'s. For evaluating $B(E2)$'s, the standard value of effective charges, i.e. $1.5e$ for protons and $0.5e$ for neutrons have been used, whereas $B(M1)$'s have been calculated by using the free values for the g_l and the free values damped by a 0.75 factor for g_s . These values are kept constant for all the isotones without any individual adjustments. One may note that very less information was reported on experimental front on these reduced transition probabilities for these nuclei; however, employing PSM wave function, the data on reduced transition

Table 1. The calculated $B(M1 \downarrow)$ values (in μ_N^2) for yrast band of $N = 45$ and $N = 46$ isotones in comparison with the available experimental and other theoretical data [7, 8, 55, 63].

^{76}Ga		^{78}As			^{80}Br		
Transition	$B(M1 \downarrow)$	Transition	$B(M1 \downarrow)$		Transition	$B(M1 \downarrow)$	
			Expt [7]	PSM		Expt [8]	PSM
$4^+ \rightarrow 3^+$	0.0120	$4^- \rightarrow 3^-$	0.06802	0.0208	$6^+ \rightarrow 5^+$	—	0.0259
$5^+ \rightarrow 4^+$	0.0844	$5^- \rightarrow 4^-$	0.0034	0.0011	$7^+ \rightarrow 6^+$	—	0.0123
$6^+ \rightarrow 5^+$	0.0704	$6^- \rightarrow 5^-$	—	0.3821	$8^+ \rightarrow 7^+$	—	0.0148
$7^+ \rightarrow 6^+$	0.0858	$7^- \rightarrow 6^-$	—	0.0507	$9^+ \rightarrow 8^+$	—	0.0107
$8^+ \rightarrow 7^+$	0.0288	$8^- \rightarrow 7^-$	—	0.0001	$10^+ \rightarrow 9^+$	0.293 ± 0.0932	0.0930
$9^+ \rightarrow 8^+$	0.0694	$9^- \rightarrow 8^-$	—	0.0310	$11^+ \rightarrow 10^+$	0.2958 ± 0.1181	0.0590
$10^+ \rightarrow 9^+$	0.0237	$10^- \rightarrow 9^-$	—	0.0163	$12^+ \rightarrow 11^+$	—	0.0618
$11^+ \rightarrow 10^+$	0.0489	$11^- \rightarrow 10^-$	—	0.0079	$13^+ \rightarrow 12^+$	—	0.0086
$12^+ \rightarrow 11^+$	0.0297	$12^- \rightarrow 11^-$	—	0.0085	$14^+ \rightarrow 13^+$	—	0.0006
$13^+ \rightarrow 12^+$	0.0065	$13^- \rightarrow 12^-$	—	0.0013			
$14^+ \rightarrow 13^+$	0.0265	$14^- \rightarrow 13^-$	—	0.0003			
^{77}Ga		^{79}As		^{81}Br			
Transition	$B(M1 \downarrow)$	Transition	$B(M1 \downarrow)$	Transition	$B(M1 \downarrow)$		
					Expt. [55]	Expt. [63]	PSM
$5/2^- \rightarrow 3/2^-$	0.1740	$5/2^- \rightarrow 3/2^-$	0.6851	$5/2^- \rightarrow 3/2^-$	0.189 ± 0.026	0.00609 ± 0.00358	0.02677
$7/2^- \rightarrow 5/2^-$	1.2073	$7/2^- \rightarrow 5/2^-$	1.1017	$7/2^- \rightarrow 5/2^-$	0.1449 ± 0.0107	0.2506 ± 0.0716	0.3090
$9/2^- \rightarrow 7/2^-$	0.4226	$9/2^- \rightarrow 7/2^-$	0.2817	$9/2^- \rightarrow 7/2^-$			0.1822
$11/2^- \rightarrow 9/2^-$	0.5158	$11/2^- \rightarrow 9/2^-$	0.3735	$11/2^- \rightarrow 9/2^-$			0.2795
$13/2^- \rightarrow 11/2^-$	0.8171	$13/2^- \rightarrow 11/2^-$	0.7257	$13/2^- \rightarrow 11/2^-$			0.5589
$15/2^- \rightarrow 13/2^-$	0.0999	$15/2^- \rightarrow 13/2^-$	0.2197	$15/2^- \rightarrow 13/2^-$			0.1749
$17/2^- \rightarrow 15/2^-$	0.7740	$17/2^- \rightarrow 15/2^-$	1.2174	$17/2^- \rightarrow 15/2^-$			1.0545
$19/2^- \rightarrow 17/2^-$	0.3745	$19/2^- \rightarrow 17/2^-$	0.2691	$19/2^- \rightarrow 17/2^-$			0.2075
$21/2^- \rightarrow 19/2^-$	1.0125	$21/2^- \rightarrow 19/2^-$	1.6913	$21/2^- \rightarrow 19/2^-$			1.6333

Table 2. The calculated $B(E2\downarrow)$ values (in e^2b^2) for yrast band of $N = 45$ and $N = 46$ isotones in comparison with the available experimental and other theoretical data [7, 8, 55, 63].

^{76}Ga		^{78}As			^{80}Br		
Transition	$B(E2\downarrow)$	Transition	$B(E2\downarrow)$		Transition	$B(E2\downarrow)$	
			Expt [7]	PSM		Expt [8]	PSM
$4^+ \rightarrow 2^+$	0.00062	$4^- \rightarrow 2^-$	0.00944	0.00792	$6^+ \rightarrow 4^+$	—	0.02459
$5^+ \rightarrow 3^+$	0.00356	$5^- \rightarrow 3^-$	0.00452	0.00484	$7^+ \rightarrow 5^+$	—	0.04060
$6^+ \rightarrow 4^+$	0.00392	$6^- \rightarrow 4^-$	—	0.00824	$8^+ \rightarrow 6^+$	—	0.05230
$7^+ \rightarrow 5^+$	0.01150	$7^- \rightarrow 5^-$	—	0.00988	$9^+ \rightarrow 7^+$	—	0.06430
$8^+ \rightarrow 6^+$	0.00781	$8^- \rightarrow 6^-$	—	0.02580	$10^+ \rightarrow 8^+$	$0.0412^{0.015}_{0.01}$	0.06413
$9^+ \rightarrow 7^+$	0.00991	$9^- \rightarrow 7^-$	—	0.03460	$11^+ \rightarrow 9^+$	$0.02070^{0.0138}_{0.0059}$	0.06040
$10^+ \rightarrow 8^+$	0.00619	$10^- \rightarrow 8^-$	—	0.03067	$12^+ \rightarrow 10^+$	$0.01973^{0.00549}_{0.00488}$	0.04030
$11^+ \rightarrow 9^+$	0.00768	$11^- \rightarrow 9^-$	—	0.03190	$13^+ \rightarrow 11^+$	—	0.06505
$12^+ \rightarrow 10^+$	0.00489	$12^- \rightarrow 10^-$	—	0.03048	$14^+ \rightarrow 12^+$	—	0.03628
$13^+ \rightarrow 11^+$	0.00599	$13^- \rightarrow 11^-$	—	0.02895			
$14^+ \rightarrow 12^+$	0.00971	$14^- \rightarrow 12^-$	—	0.02630			

^{77}Ga		^{79}As		^{81}Br		
Transition	$B(E2\downarrow)$	Transition	$B(E2\downarrow)$	Transition	$B(E2\downarrow)$	
					Expt [55]	Expt. [63]
$7/2^- \rightarrow 3/2^-$	0.03281	$7/2^- \rightarrow 3/2^-$	0.03471	$7/2^- \rightarrow 3/2^-$	0.03515 ± 0.002	0.02978 ± 0.00248
$9/2^- \rightarrow 5/2^-$	0.06999	$9/2^- \rightarrow 5/2^-$	0.07019	$9/2^- \rightarrow 5/2^-$		
$11/2^- \rightarrow 7/2^-$	0.05593	$11/2^- \rightarrow 7/2^-$	0.06183	$11/2^- \rightarrow 7/2^-$		
$13/2^- \rightarrow 9/2^-$	0.07503	$13/2^- \rightarrow 9/2^-$	0.07632	$13/2^- \rightarrow 9/2^-$		
$15/2^- \rightarrow 11/2^-$	0.04854	$15/2^- \rightarrow 11/2^-$	0.00002	$15/2^- \rightarrow 11/2^-$		
$17/2^- \rightarrow 13/2^-$	0.07763	$17/2^- \rightarrow 13/2^-$	0.07784	$17/2^- \rightarrow 13/2^-$		
$19/2^- \rightarrow 15/2^-$	0.02423	$19/2^- \rightarrow 15/2^-$	0.00695	$19/2^- \rightarrow 15/2^-$		
$21/2^- \rightarrow 17/2^-$	0.06329	$21/2^- \rightarrow 17/2^-$	0.06535	$21/2^- \rightarrow 17/2^-$		

probabilities has been obtained for the yrast energy states up to the spin of $16\hbar$ in odd–odd $N = 45$ isotones and $21/2^-$ for odd- Z $N = 46$ isotones.

On the experimental front, no data is available for ^{76}Ga , while for ^{78}As $B(M1)$ values are available for only $4^- \rightarrow 3^-$ and $5^- \rightarrow 4^-$ transitions [7]. The values predicted by PSM for the $4^- \rightarrow 3^-$ transition is less than the experimental values by about 0.04 unit but for $5^- \rightarrow 4^-$ transition the difference is of just 0.002 units. In case of ^{80}Br , again the experimental data [8] is available for two transitions ($10^+ \rightarrow 9^+$ and $11^+ \rightarrow 10^+$) only. However, in this case there is a little divergence of the PSM results from the experimental data. This discrepancy may be overcome if we change the damping factor for g_s or if we include in our calculations the higher configurations (e.g. $4\text{-}qp$). As already mentioned, we wanted to keep our parameters fixed so we did not go for individual adjustment of the damping factor for this particular nucleus and as far as configuration space is concerned, this is the drawback in the present setup of the PSM that our calculations for odd–odd nuclei are limited to $2\text{-}qp$ configurations only. We will try to fix this in the near future but for the present paper, we decided to keep ourselves restricted as the essence of physics is still well understood. In case of $N = 46$ isotones, the experimental $B(M1)$'s are available only for ^{81}Br [55, 63]. For this nucleus, our results are more close to the data available from the Nuclear data sheets [63] and follow the same trend in contrast to the experimental data predicted by Jakob *et al* [55].

If we talk about $B(E2)$ transition probabilities, experimental data is available for only ^{78}As [7], ^{80}Br [8] and ^{81}Br [55, 63], that too for just few transitions. While the PSM results are very close to the experimental ones in case of ^{78}As and ^{81}Br , for ^{80}Br , there is a slight discrepancy. If we change the value of effective charge here, this discrepancy could be resolved to some extent but again we did not want to make individual adjustments so the results are presented as they are. An overall satisfactory degree of agreement is obtained between the experimental and the PSM data for the reduced transition probabilities. The new data predicted by the PSM calculations for these properties is open for the further experimental verification.

4. Conclusions

In contrast to even–even nuclei, the calculations reveal that odd–odd nuclei have coexisting low-lying two-quasiparticle states, i.e. in odd–odd nuclei, the energy differences between low-lying $2\text{-}qp$ states is very small, e.g. less than 100 keV which makes it difficult to understand their intricate structure. In order to gain better knowledge of the structure of the odd–odd nuclei, particularly those lying in mass-70 region, PSM calculations have been performed on $N = 45$ isotones. In addition to these doubly-odd isotones, some neighbouring $N = 46$ odd-mass (odd- Z) isotones have also been studied to check the efficacy of the PSM Hamiltonian to give the unified description of nuclei lying in a particular mass region of the Segre chart. The calculated data reproduces reasonably well the reported experimental data on the yrast bands and predicted the high spin states in these nuclei, where current data are still sparse. Attempt has been made to understand their intricate structure from the band diagrams and it is observed that the proton orbitals $f_{5/2}$ and $g_{9/2}$ and neutron orbitals $p_{3/2}$, $f_{5/2}$ and $g_{9/2}$ play crucial role in deciding the band structure of doubly-odd $N = 46$ isotones and are also responsible for the changing spin and parity of the band-head of the ground state band as we move from ^{76}Ga to ^{78}As to ^{80}Br . In case of $N = 46$ isotones, proton orbitals $f_{7/2}$ and $f_{5/2}$ are important whereas the neutron orbital $g_{9/2}$ is dominant in deciding their structure. The phenomena of signature splitting and inversion are also studied and the role of the $\pi g_{9/2} \otimes \nu g_{9/2}$ configuration in producing the inversion of signature around the spin $11\hbar$ is

also established through present calculations. The experimental results on the rotational alignments, kinematical and dynamical moments of inertia are also very well reproduced by our calculations and these properties were studied within the context of the band crossings. Further, predictions on reduced $B(M1)$ and $B(E2)$ transition probabilities have been made in the present work. One may note that prior to the present work, very little information was available concerning the $B(M1)$'s and $B(E2)$'s of yrast bands in these nuclei so, more experimental data is sought for the complete description of such nuclei in the near future.

Acknowledgments

One of the authors, SKK, acknowledges the financial support from Council of Scientific and Industrial Research (CSIR), Govt. of India, under sanction no. 03(1424)/18/EMR-II.

The authors of the present paper also express their gratitude to Prof Y Sun and Prof J A Sheikh for their suggestions.

ORCID iDs

Suram Singh  <https://orcid.org/0000-0002-7545-3384>

References

- [1] Nazarewicz W, Dudek J, Bengtsson R, Bengtsson T and Ragnarsson I 1985 *Nucl. Phys. A* **435** 397
- [2] Chuangye He *et al* 2013 *Phys. Rev. C* **87** 034320
- [3] Sun Y, Yang Y C, Jin H, Kaneko K and Tazaki S 2012 *Phys. Rev. C* **85** 054307
- [4] Mane E *et al* 2011 *Phys. Rev. C* **84** 024303
- [5] Doring J *et al* 1991 *Z. Phys. A* **339** 425
- [6] Doring J *et al* 1984 *Z. Phys. A* **316** 75
- [7] Doring J *et al* 1996 *Z. Phys. A* **354** 345
- [8] Ray I *et al* 2000 *Nucl. Phys. A* **678** 258
- [9] Doring J, Ulrich D, Johns G D, Riley M A and Tabor S L 1999 *Phys. Rev. C* **59** 71
- [10] Petrovici A, Schmid K W, Radu O and Faessler A 2006 *Eur. Phys. J. A* **28** 19
- [11] Dombos A C *et al* 2016 *Phys. Rev. C* **93** 064317
- [12] Singh B and Farhan A R 2006 *Nucl. Data Sheets* **107** 1923
- [13] Shui-Fa S *et al* 2006 *High Energy Phys. Nucl. Phys.* **30** 1234
- [14] Wang S Y *et al* 2011 *Phys. Lett. B* **703** 40
- [15] Singh B 1995 *Nucl. Data Sheets* **74** 63
- [16] Farhan A R and Singh B 2009 *Nucl. Data Sheets* **110** 1917
- [17] Singh B 2005 *Nucl. Data Sheets* **105** 223
- [18] Otsuka T *et al* 2005 *Phys. Rev. Lett.* **95** 232502
- [19] Otsuka T *et al* 2010 *Phys. Rev. Lett.* **104** 012501
- [20] Kaneko K, Mizusaki T, Sun Y and Tazaki S 2015 *Phys. Rev. C* **92** 044331
- [21] Plettner C *et al* 2000 *Phys. Rev. Lett.* **85** 2454
- [22] Rainovski G *et al* 2002 *J. Phys. G: Nucl. Part. Phys.* **28** 2617
- [23] Jenkins D G *et al* 2002 *Phys. Rev. C* **65** 064307
- [24] Petrovici A, Schmid K W and Faessler A 2002 *Nucl. Phys. A* **710** 246
- [25] Petrovici A, Schmid K W and Faessler A 2002 *Nucl. Phys. A* **708** 190
- [26] Petrovici A, Schmid K W, Grummer F and Faessler A 1990 *Nucl. Phys. A* **517** 108
- [27] Srivastava P C 2012 *J. Phys. G: Nucl. Part. Phys.* **39** 015102
- [28] Johns G D, Doring J, Kaye R A, Sylvam G N and Tabor S L 1997 *Phys. Rev. C* **55** 660
- [29] Chaudhary R, Makhnotra N K, Devi R and Khosa S K 2015 *Nucl. Phys. A* **939** 1
- [30] Dar P A, Verma S, Devi R and Khosa S K 2008 *Pramana* **70** 817
- [31] Dar P A, Devi R, Khosa S K and Sheikh J A 2007 *Phys. Rev. C* **75** 054315
- [32] Verma S, Devi R and Khosa S K 2006 *Eur. Phys. J. A* **30** 531

- [33] Dar P A, Verma S, Devi R and Khosa S K 2008 *Pramana* **70** 817
- [34] Verma P *et al* 2013 *Nucl. Phys. A* **918** 1
- [35] Gupta A *et al* 2015 *Nucl. Phys. A* **941** 48
- [36] Verma P, Sharma C, Singh S, Bharti A and Khosa S K 2012 *Nucl. Phys. A* **884** 1
- [37] Sharma C, Verma P, Singh S, Bharti A and Khosa S K 2012 *Eur. Phys. J. A* **48** 138
- [38] Verma P, Sharma C, Singh S, Bharti A and Khosa S K 2013 *AIP Conf. Proc.* **1524** 101
- [39] Kaye R A *et al* 2011 *Phys. Rev. C* **83** 044316
- [40] Stefanescu I *et al* 2004 *Phys. Rev. C* **70** 044304
- [41] Kaneko K *et al* 2010 *Phys. Rev. C* **82** 061301
- [42] Hasegawa M, Kaneko K and Mizusaki T 2005 *Phys. Rev. C* **72** 064320
- [43] Badica T *et al* 2009 *Rom. J. Phys.* **54** 467
- [44] Sohlér D *et al* 1997 *Nucl. Phys. A* **618** 35
- [45] Brant S, Yoshida N and Zuffi L 2004 *Phys. Rev. C* **70** 054301
- [46] Kumar S *et al* 2014 *Phys. Rev. C* **89** 034303
- [47] Palit R, Sheikh J A, Sun Y and Jain H C 2003 *Phys. Rev. C* **67** 014321
- [48] Flanagan *et al* 2010 *Phys. Rev. C* **82** 041302
- [49] Hara K and Sun Y 1995 *Int. J. Mod. Phys. E* **4** 637
- [50] Ring P and Schuck P 1980 *The Nuclear Many-Body Problem* (New York: Springer)
- [51] Zhang J Y, Larabee A J and Reidinger L L 1987 *J. Phys. G: Nucl. Phys.* **13** L75
- [52] Dieterich W, Bäcklin A, Lannergård C O and Ragnarsson I 1975 *Nucl. Phys. A* **253** 429
- [53] Moller P, Nix J R, Myers W D and Swiatecki W J 1995 *At. Data Nucl. Data Tables* **59** 185
- [54] Seewald *et al* 1998 *Phys. Rev. Lett.* **80** 5289
- [55] Jakob G *et al* 1996 *Nucl. Phys. A* **601** 117
- [56] Sun Y and Egido J L 1994 *Nucl. Phys. A* **580** 1
- [57] Castel B and Towner I S 1990 *Modern Theories of Nuclear Moments* (Oxford: Clarendon)
- [58] Singh B 2012 *Nucl. Data Sheets* **113** 115
- [59] Singh B 2002 *Nucl. Data Sheets* **96** 1
- [60] Baglin C M 2008 *Nucl. Data Sheets* **106** 2257
- [61] Rab S 1991 *Nucl. Data Sheets* **63** 1
- [62] Shen S *et al* 2010 *Phys. Rev. C* **82** 014306
- [63] Baglin C M 1993 *Nucl. Data Sheets* **69** 267